An Earlier Lidar Observation of a Noctilucent Cloud above Logan, Utah (41.7º N, 111.8º W)

Joshua P. Herron and Vincent B. Wickwar
Center for Atmospheric and Space Sciences, Utah State University, Logan, UT, USA

Abstract. A Rayleigh-scatter lidar has been operated at the Atmospheric Lidar Observatory (ALO) on the Utah State University (USU) campus (41.7º N, 111.8º W) for the last 11 years. During the morning of 22 June 1995 a noctilucent cloud (NLC) was observed with the lidar, for approximately one hour, well away from the twilight periods when NLCs are visible. This sighting of an NLC at this latitude shows that the first sighting in 1999 [*Wickwar et al.*, 2002] was not a unique occurrence. This 1995 observation differs from the 1999 one in that temperatures could be deduced. The hourly profiles are at least 20 K cooler than the 11-year June climatology for ALO near the NLC altitude. However, the cool temperatures arose because of a major temperature oscillation or wave, not because the whole profile was cooler. These lidar observations were supplemented by OH rotational observations from approximately 87 km, which also showed unusually cold temperatures on this night. While these NLC observations equatorward of 50° may be significant harbingers of global change, the mechanism is more complicated than a simple overall cooling or increase in water vapor.

Index terms: 0305 Atmospheric Composition and Structure: Aerosols and particles (0345,4801); 0320 Atmospheric Composition and Structure: Cloud physics and chemistry: 0340 Atmospheric Composition and Structure: Middle atmosphere–composition and chemistry; 3384 Meteorology and Atmosphere Dynamics: Waves and tides; *Keywords*: noctilucent clouds, summer mesosphere, Rayleigh lidar, global change.

Introduction

Noctilucent clouds (NLCs) typically occur during the summer months at between 80 and 86 km [*Gadsden and Schroder*, 1989; *Thomas and Olivero*, 1989] in the polar regions at latitudes greater than 50°. They most likely consist of ice particles [*von Cossart et al.*, 1999; *Hervig et al.*, 2001]. NLC observations are important because they give the longest record of trends in the middle atmosphere and are sensitive to global change. Lidar observations of NLCs give information about the exact altitude of the NLC and its variability. Recently several summaries of NLC observations have been compiled [*Chu et al.*, 2003; *Collins et al.*, 2003; *Fiedler et al.*, 2003; *Thayer et al.*, 2003]. The first reported NLC observed below 50° was reported by the ALO lidar group in 1999. Because of concern that this observation was not the first one, the entire database was analyzed looking for additional NLCs. A second event was found four years earlier than the reported event.

Observational Technique

The Rayleigh-scatter lidar at ALO is located in Logan, UT (41.7º N, 111.8º E) on the Utah State University (USU) campus approximately 1.46 km above sea level. The ALO Rayleigh-scatter lidar has been in operation since 1993. The lidar has been operated whenever possible over the last 11 years and a database of nightly relative-density profiles and absolute temperatures have been compiled.

The ALO Rayleigh-scatter lidar is a coaxial system with a power aperture product to 3.3 W-m^2. The system is composed of a Spectra Physics Nd:YAG laser operating at 30 Hz generating 20-22

watts at 532 nm and a 44-cm diameter Newtonian telescope. The signals from below ~18 km are blocked by a mechanical chopper and the gain is reduced by almost 1000 by an electronic gate below 38 km. A narrow-band interference filter is used to remove most of the background light, and good data are acquired above 45 km. The gated detector is a green-sensitive, bi-alkali photomultiplier tube (Electron Tubes 9954B) in a Peltier-cooled housing. A more extensive description of this system is given in [*Wickwar et al.*, 2001]. The sampling gate width is 250 ns giving an altitude resolution of 37.5 m. The returns from 3600 pulses are integrated together in the data acquisition system giving a time resolution of 2 minutes.

Observations

During the morning of 22 June 1995 the lidar was operated from 6:31 UT (00:31 MDT) until 10:55 UT (04:55 MDT). An enhancement in the photocount profiles was observed with the Rayleigh-scatter lidar between 7:54 UT and 8:48 UT with a shorter enhancement occurring at 09:25 to 09:40 UT. This time period corresponded to solar depression angles from 21.5º to 11.2º, giving shadow heights from ~450 to 120 km. Accordingly the cloud was not scattering sunlight, but we still take the liberty of calling it an "NLC."

The lidar photocount profiles usually consist of the Rayleigh-scattered photons, which are proportional to density, background light, and thermionic emission or darkcount from the photomultiplier tube. When an NLC is present there is an additional component from Mie-scatter, which is seen as an enhancement in the photocount profile. The enhancement in the lidar profile is clearly shown in the left side of Figure 1. The signal from the peak of the layer is equivalent to the Rayleigh-scatter signal at an altitude of ~ 70 km.

The backscatter ratio $R(z)$ is used as a measure of the NLC strength. It is the ratio of the measured signal $S(z)$ to the Rayleigh-scattered signal $S_R(z)$:

$$R(z) = \frac{S(z)}{S_R(z)} = \frac{S_r(z) + S_m(z)}{S_R(z)} \tag{1}$$

where S_M is the backscattered signal from Mie scatter. A 2-D boxcar average was applied to the Rayleigh-scatter returns to reduce the noise level, but this also smoothed over the NLC parameters. The averaging was only carried out over 6 points in time and 4 points in altitude, corresponding to 12 minutes and 150 meters, to minimize the effect of the averaging. The profile for the Rayleigh-scattered signal S_R used to calculate the backscatter ratio R in Equation 1 was found by averaging all the periods during the night of 22 June without evidence of the NLC. To eliminate the possibility of contamination by Mie-scatter a 3rd order polynomial was used to approximate the Rayleigh-scattered signal in the region of the NLC. This was accomplished by using the natural log of the data from 3 km above the NLC and 3 km below. This fitted profile and the measured profile were used to calculate the backscatter ratio. The fitted and unfitted profiles give equivalent results. The right side of Figure 1 shows the backscatter ratio from the unfitted profile.

The maximum backscatter value of 8.2 occurred at UT, and is the profile shown on the right side of Figure 1. Similar profiles calculated every 2 minutes were used to create a contour plot of the backscatter ratio Figure 2. The main body of the NLC occurred between 7:54 and 8:48 UT. In addition to the main body, a small enhancement in the backscatter ratio occurred between 9:25

and 9:40 UT at ~83 km. The peak of the NLC layer does not remain at the same altitude. The phase progression of the peak has an apparent downward velocity of .96 km/hr or 27 cm/s similar to other NLC observations [*Collins et al.*, 2003]. The main body of the NLC shows an apparent descent rate of -1.9 km/hr. This value was found by a linear fit to the time variation of the peak altitude.

At the height of the NLC, the diameter of the laser beam is ~40 m. This small field of view means that we are sampling a small portion of the cloud. The field of view is also fixed in the zenith direction preventing any knowledge of the horizontal extent or structure of the cloud. As such it is not possible to distinguish between a layer descending into the beam and a slanted layer being transported horizontally across the beam.

Two differences between this 1995 observation and the 1999 observation are that the laser had more power and the background signal was well behaved. The latter is extremely important for deriving temperatures [*Herron and Wickwar*, 2005]. Assuming hydrostatic equilibrium and the ideal gas law, the temperatures can then be derived from measurements of relative density. As previously stated the Rayleigh-scattered photons are proportional to density. However, the Mie-scatter enhancement from the NLC isn't, and must be removed to derive the temperature profile.

The individual two minute profiles are averaged together into three periods. The first period spans from the start of observations for the night to shortly before the start of the NLC. The second encompasses the NLC, and the third spans from after the NLC to shortly before dawn. The first and third periods have no NLC enhancement and were used to examine fitting routines for the second period. Several low order polynomials were fitted to 81 points above and 81 points below the NLC region. A 3rd order polynomial fitted the log of the average photocount profile produced the lowest Chi^2 values. The results of the fit are used to replace the data in the NLC region. These curves are then smoothed in altitude with a running boxcar average over 81 points (3 km) and the results used to calculate the relative density profile. The first two relative density profiles are shown in Figures 3(a) and (b). The red curves are the observed profiles and the black profiles containing the fits. In the first profile is almost linear in the semi-log plot. In contrast, in the second hour, there is an apparent density enhancement, a bump on the straight line, due to the NLC. The fitted profiles are then used to calculate the corresponding temperature profiles. To our knowledge, this is the first time Rayleigh-scatter temperatures have been derived in the vicinity of a NLC. However, steps in this direction have been taken by others. Collins et al. [2003] interpolated over the NLC layer to calculate the backscatter ratio. *Lübken et al.* [1996] interpolated lidar measurements across the NLC region to find the molecular signal for calculating the backscatter ratio when additional density measurements were not available from falling spheres. *Stebel et al.* [2004] interpolated across a possible wintertime aerosol layer to calculate Rayleigh temperatures.

To derive absolute temperatures from the relative density profiles a "best guess" temperature is needed at the highest altitude. The highest altitude is determined to be is the point where the signal has dropped to 20σ, where σ is the measurement uncertainty based on the photon statistics. The value used for that was taken from the temperature climatology from the Colorado State University (CSU) sodium lidar [*She et al.*, 2000]. While this is a climatological value, it is still the best source available for a particular night. The temperature profiles for the three periods are

shown in Figure 4. The minimum temperatures for all three profiles are found between 82 and 87 km. The second and third profiles reached a minimum value of ~150 K in this region. The first period was warmer with a minimum of ~ 157 K.

A comparison of these temperature profiles to the June average from the ALO Rayleigh lidar climatology shows the general magnitude of the temperature departures, Figure 5. From 80 and 88 km the temperatures are between 10 and 23 K cooler than the June average. In addition to the cooling at the NLC altitudes the temperatures from 65 and 80 km are warmer than the June average and the maximum value is ~ 17 K above the June average. The departures from the June average are apparently the effects of a large temperature oscillation.

To re-enforce the temperature measurements made with the Rayleigh lidar additional temperature measurements were desirable. A BOMEM Michelson interferometer was in operation at USU during the same night that the NLC was observed [*Espy*, 2003]. The temperature values are derived from observations of the rotational structure of the (3,1) Meinel band from the OH airglow centered at ~87 km. Temperature measurements made during the month of June in both 1995 and 1996, along with the ALO temperatures from June 1995 at 87 km, are shown in Figure 6. Because of uncertainties in the OH transition probabilities, the rotational temperatures from the BOMEM and the kinetic temperatures from the lidar cannot be directly compared, but the relative variations are reliable.

As illustrated in Figure 6 the all-night temperature for 22 June 1995 is significantly cooler than for the other nights. In addition to the very cool night for 22 June 1995, the temperature values from 1995 are themselves cooler than from 1996. In particular the temperatures from 20 to 26 June 1995 are consistently cooler. While the initial starting point for the lidar reduction between 88 and 91 km. The temperature measurements from the lidar showed the 22nd to be the coolest night during June of 1995. The starting altitudes for these nightly temperatures are between 88 and 91 km only slightly above 87 km. The temperatures at 87 km are strongly influenced by the initial temperature as a uncertainty of ±5 K is reduced to ±3.5 K after 2 km of integration.

Temperature measurements from the BOMEM are available on sub hour intervals and the results for 22 June 1995 are shown in Figure 7. The temperatures dropped quickly after 0500 UT to a minimum at 0600 UT. Other relative minima occurred at 0715, 0930, and 1040 UT showing a temporal oscillation in the OH temperatures. With the OH layer centered at ~87 km these temperature measurements are above the altitude of the NLC layer. The lowest temperatures were observed well before the appearance of the NLC in the lidar returns at 0800 UT. The NLC particles most like formed in this cold region and were only detectable the lidar after some growth and sedimentation occurred accounting for its appearance at a later time and a lower altitude.

Discussion

At higher altitudes the necessary temperatures for NLC formation is found at or near the mesopause [Thomas, 1996]. At mid latitudes the average mesopause temperature is not low enough for the formation of NLCs. The mean temperature measured with the ALO Rayleigh-scatter lidar at 85 km during June is ~ 170 K. This value is significantly higher than what is typical seen around NLCs (135 K) [*Lübken et al.*, 1996]. The presence of an NLC at these

latitudes therefore must be a product of some other process than just a general atmospheric cooling. The comparison of the three temperature profiles to the June climatology shows a large temperature oscillation or wave. A large oscillation was also observed in the OH temperatures during the course of the night. We believe that this temperature oscillation is responsible for driving the temperature down to ~150 K at the NLC altitude.

One possible source for the observed oscillation is the atmospheric tide. During the summer period phasing of the tide is such that at the altitude of the NLC a minimum occurs shortly after local midnight. This minimum in the diurnal tide is observable in the tides derived from the mid-latitude sodium lidars [*States and Gardner*, 2000; *She et al.*, 2002] and in atmospheric models such as GSWM [*Hagan et al.*, 1999; *Hagan et al.*, 2001].Figure 8 shows the minimum in the diurnal tide with respect to the NLC altitude and Figure 9 shows the combined semi-diurnal and diurnal tides.

The phasing of the diurnal component of the CSU results gives a descent rate for the tide of ~.74 km/hr corresponding to a vertical wavelength of ~ 17.7 km. The maximum value for each vertical profile of backscatter ratio was fit with a linear regression and the resulting descent rate is ~0.96 km/hr. The descent rate of the NLC is faster than the observed diurnal tide and may be a result of sedimentation, the influence of a semi-diurnal component, or the effects of a slanted NLC layer. In addition to the difference in the descent rates the magnitude of the temperature oscillation is much larger than the average diurnal tide and suggests an enhancement of the diurnal tide.

The minimum temperature was observed by the BOMEM shortly after local midnight at approximately 87 km. In comparison the minimum temperature observed with the lidar was observed 2.5 hours later at an altitude of ~ 85 km giving a descent rate of ~.8 km/hr. This rate is close to the descent rate of the diurnal tide seen with the CSU lidar suggesting that the minimum is following the tide.

To better compare the two NLC observations made with the ALO lidar the results from the 1999 NLC were re-analyzed using the same temporal and vertical averaging as the 1995 NLC, Figure 10. The magnitudes of both NLCs were weak when compared to those observed at higher latitudes where the backscatter ratio can be greater than 200. The maximum value for the backscatter ratio for the 1995 NLC was almost double the maximum of 4.6 reached by the 1999 NLC.

There is a strong linear trend in the altitude of NLCs with latitude caused by differences in the temperature structure of the mesopause. The 1999 NLC shows a mean altitude of 82.1 km which is in very good agreement with the linear trend [*Chu et al.*, 2004]. The mean height of the 1995 NLC was 83.6 km, a difference of 1.7 km.

The middle atmosphere is relatively stable, but large variations on the order of ± 20 K due to wave activity has been reported in the past at NLC altitudes [*von Zahn and Meyer*, 1989]. We propose that the large amplitude wave seen in the temperature measurements from the lidar was responsible for the formation of the NLC by driving the temperatures significantly cooler than normal.

Conclusion

We have presented results on a NLC observed at 42º N from 1995. This observation was made from a re-analysis of the ALO Rayleigh-scatter database for NLCs. While no visual observations were made we maintain that the enhancement was due to the presence of an NLC.

To date this is the second observation of an NLC below 50º and shows that the first observation wasn't an anomaly. This observation precedes the first by 4 years and its presence shows that there may be other observation of NLC at mid-latitudes. Several Rayleigh-scatter lidars are operated at equivalent latitudes and to date none have reported any NLC observation. Is there some longitudinal variation in the occurrence of NLCs at mid latitudes, e.g., its location in the Rocky Mountains?

The appearance of NLCs at latitudes < 50º N has been predicted with atmospheric models [Thomas, 1996]. These predictions follow from increases in greenhouse gasses and methane leading to a cooling in the upper mesosphere and an increase in water vapor. NLCs have been observed at 41.7º N in June of 1995 and 1999 without the significant increases in greenhouse gasses or methane the models predicted were necessary. These observations show that the mechanism for the generation of NLCs is more complicated than uniform mesospheric cooling. Could the large amplitude wave seen in the lidar temperature be a manifestation of global change, e.g., more gravity waves interacting with a tide or planetary wave?

References.

Chu, X., C. Gardner, and R.G. Roble, Lidar studies of interannual, seasonal, and diurnal variations of polar mesospheric clouds at the South Pole, *J. Geophys. Res*, *108* (D8), 8447, doi:10.1029/2002JD002524, 2003.

Chu, X., G.J. Nott, P.J. Espy, C.S. Gardner, J.C. Diettrich, M.A. Clilverd, and M.J. Jarvis, Lidar observations of polar mesospheric clouds at Rothera, Antartica (67.5^{o}S, 68.0^{o}W), *Geophys Res. Lett.*, *31* (L02114), 5, 2004.

Collins, R.L., M.C. Kelley, M.J. Nicolls, C. Ramos, T. Hou, T.E. Stern, K. Mizutani, and T. Itabe, Simultaneous lidar observations of a noctilucent cloud and an internal wave in the polar mesosphere, *Journal of Geophysical Research*, *108* (D8), 8435, 2003.

Fiedler, J., G. Baumgarten, and G. von Cossart, Noctilucent clouds above ALOMAR between 1997 and 2001: Occurrence and properties, *J. Geophys. Res*, *108* (D8), 8453, 10.1029/2002JD0035219, 2003.

Gadsden, M., and W. Schroder, *Noctilucent Clouds*, 190 pp., Springer-Verlag, New York, NY, 1989.

Hagan, M., M.D. Burrage, J.M. Forbes, J. Hackney, W.J. Randel, and X. Zhang, GSWM-98: Results for migrating solar tides, *Journal of Geophysical Research*, *104* (A4), 6813-6827, 1999.

Hagan, M., R.G. Roble, and J. Hackney, Migrating thermospheric tides, *Journal of Geophysical Research*, *106* (A7), 12739-12752, 2001.

Hervig, M., R.E. Thompson, M. McHugh, L.L. Gordley, J. Russell, and M.E. Summers, First confirmation that water ice is the primary component of polar mesospheric clouds, *Geophys Res. Lett.*, *28* (6), 971-974, 2001.

Lübken, F.-J., K.-H. Fricke, and Langer, Noctilucent clouds and the thermal structure near the Arctic mesopause in summer, *J. Geophys. Res.*, *101* (D5), 9489–9508, 17045–17046, 1996.

She, C.Y., S. Chen, B.P. Williams, Z. Hu, and D.A. Krueger, Tides in the mesopause region over Fort Collins, Colorado (41 N, 105 W) based on lidar temperature observations covering full diurnal cycles, *Journal of Geophysical Research*, *107* (D18), 12, 2002.

States, R.J., and C.S. Gardner, Thermal structure of the mesopause regioin (80–105 km) at 40°N latitude. Part II: Diurnal Variations, *J. Atmos. Sci.*, *57*, 78–92, 2000.

Thayer, J.P., M. Rapp, A.J. Gerrard, T.J. Kane, and E. Gudmundsson, Gravity-wave influences on Arctic mesospheric clouds as determined by a Rayleigh lidar at Sondrestrom, Greenland, *J. Geophys. Res*, *108* (D8), 8449, doi:1029/2002JD002363, 2003.

Thomas, G.E., and J.J. Olivero, Climatology of polar mesospheric clouds, 2. Further analysis of Solar Mesosphere Explorer data, *J. Geophys Res.*, *94*, 14673–14681, 1989.

von Cossart, G., J. Fiedler, and U. von Zahn, Size distribution of NLC particles as determined from 3-color observations of NLC by ground lidar, *Geophys. Res. Lett.*, *26* (11), 1513–1516, 1999.

von Zahn, U., and W. Meyer, Mesopause temperature in polar summer, *J. Geophys. Res.*, *94*, 14647–14651, 1989.

Wickwar, V.B., M.J. Taylor, J.P. Herron, and B.A. Martineau, Visual and lidar observations of noctilucent clouds above Logan, Utah, at 41.7°N, *J. Geophys. Res.*, *107* (D7), 10.1029/2001JD002280, 2002.

Wickwar, V.B., T.D. Wilkerson, M. Hammond, and J.P. Herron, Mesospheric temperature observations at the USU / CASS Atmospheric Lidar Observatory (ALO), in *Remote Sensing of the Atmosphere, Environment, and Space*, edited by U.N. Singh, T. Itabe, and N. Sugimoto, pp. 272-284, SPIE, 2001.

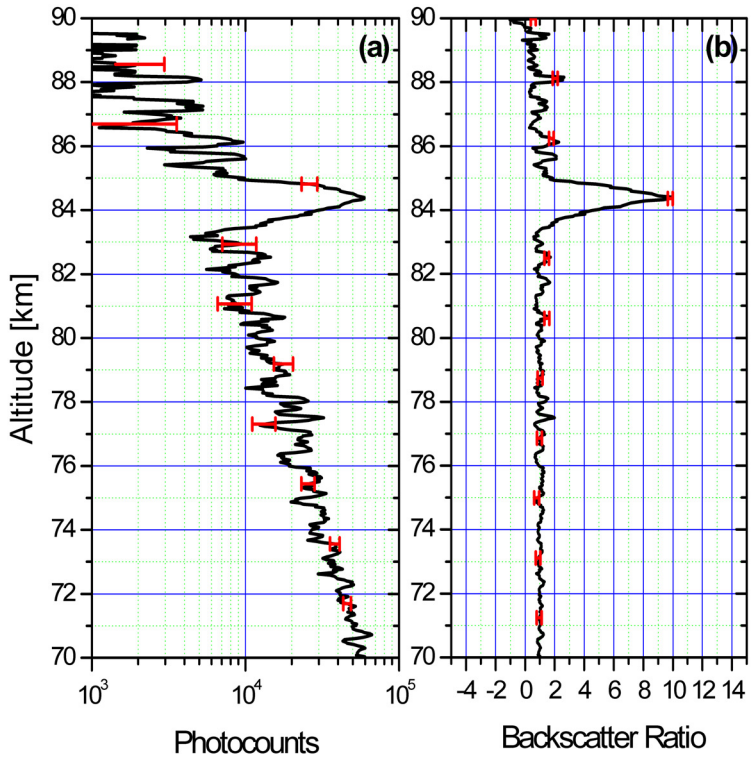

Figure 1 The left and right profiles are taken from the same 12 minute period. The left figure is the photocount profile while the right is the backscatter ratio calculated from the photocount profile. These profiles represent the peak in the observed NLC.

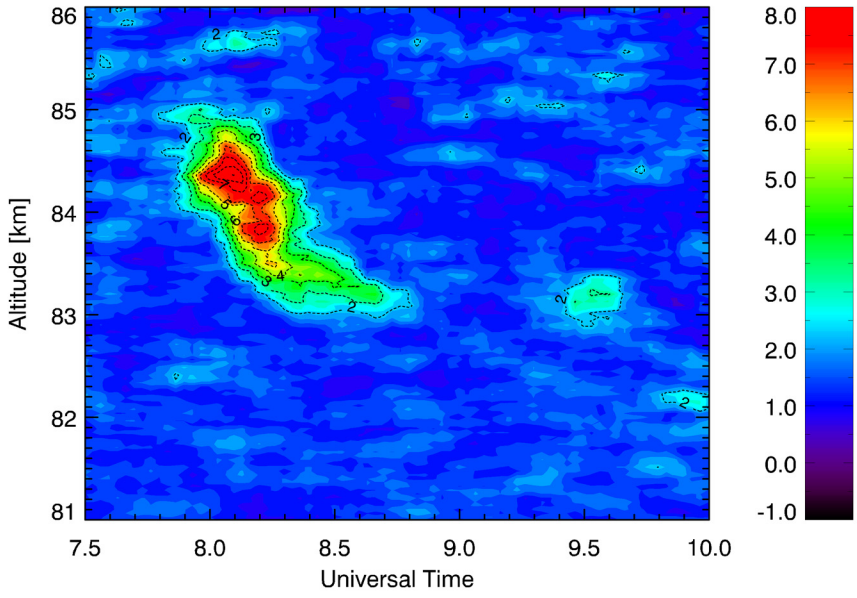

Figure 2 Contour profile of the backscatter ratio. The profiles are created from a 12 minute average in time and a 150 m average in altitude. A backscatter ratio of 1 indicates that there is no Mie-scatter enhancement.

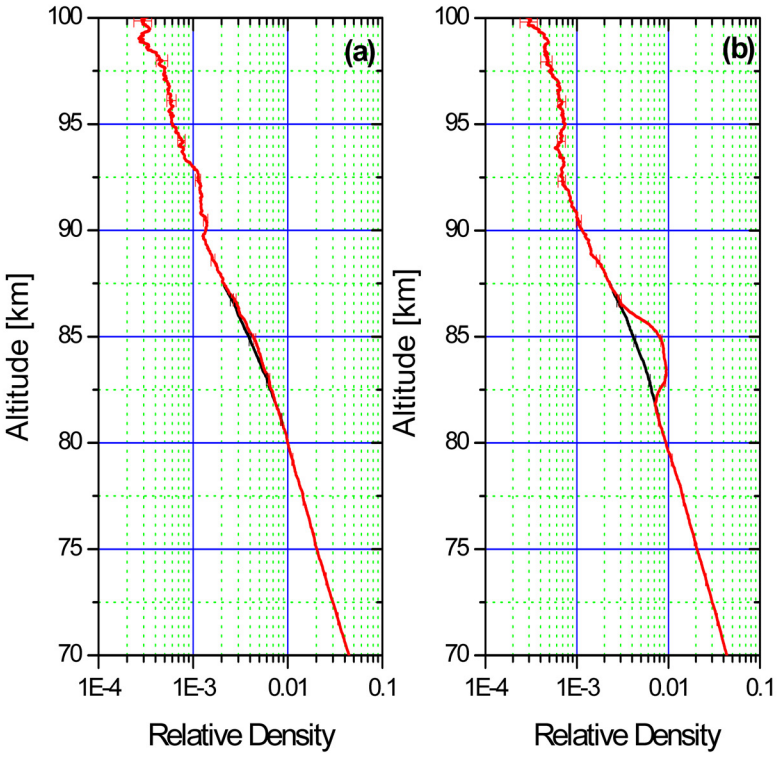

Figure 3 Relative density profiles for the first two profiles. The red curves are the measured density values with the black curve being the results of the 3rd Order polynomial fit.

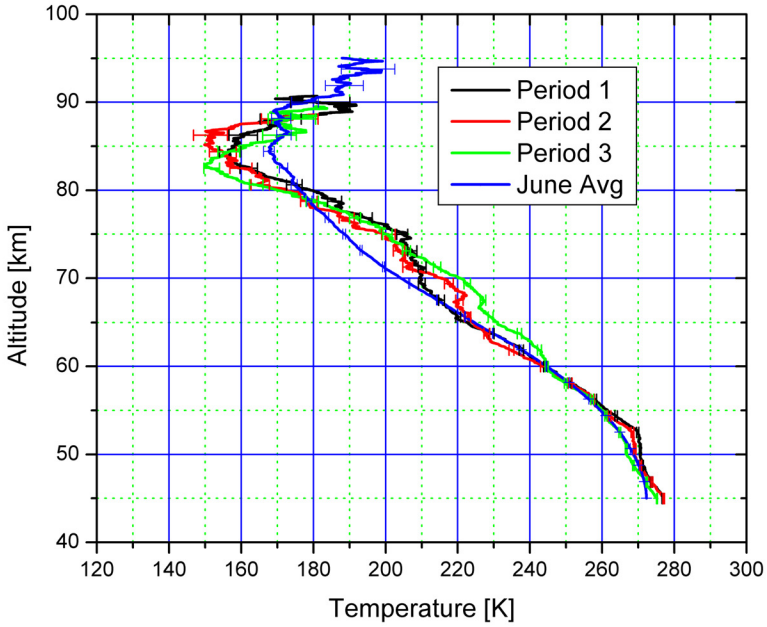

Figure 4 Temperature profiles for the three periods on June 22nd. The fourth profile is the average June temperature taken from the ALO climatology.

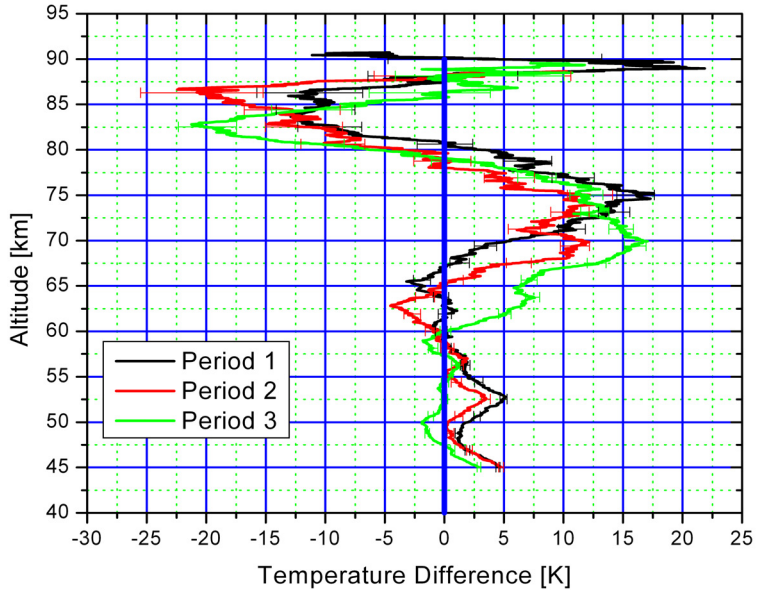

Figure 5 Temperature differences between the observed values on June 22nd and the average June temperature taken from the ALO climatology.

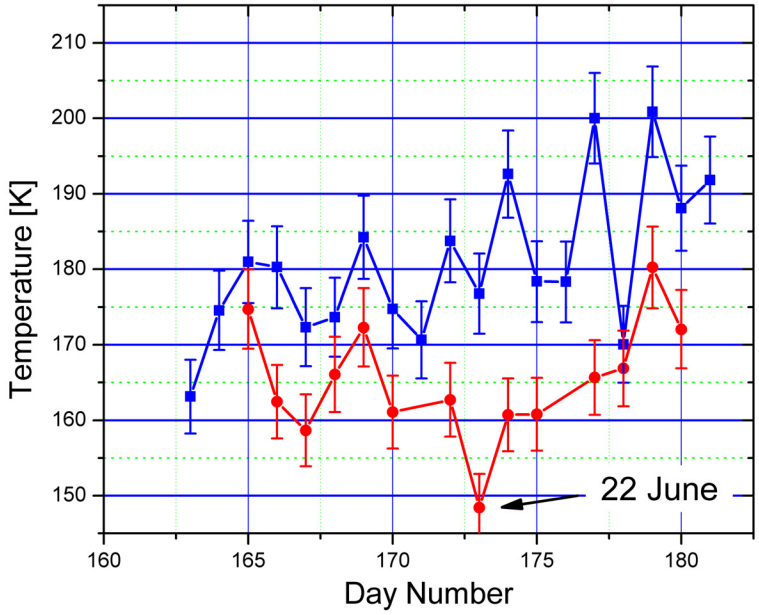

Figure 6 Oh Temperatures at 87 km from the BOMEM located at USU. The red denotes the values from 1995 and blue denotes those from 1996.

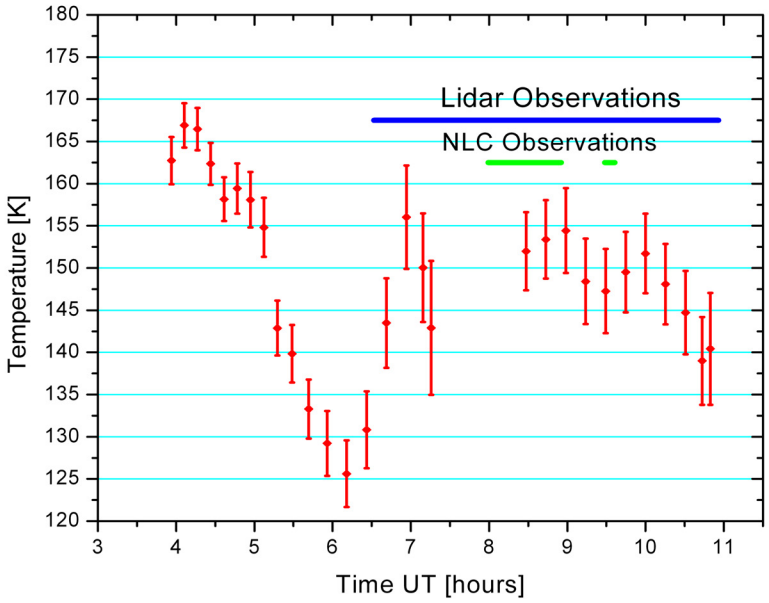

Figure 7 BOMEM OH temperatures from June 22nd are indicated in red. The period that the lidar was in operation is indicated in blue, and the NLC observations are in green.

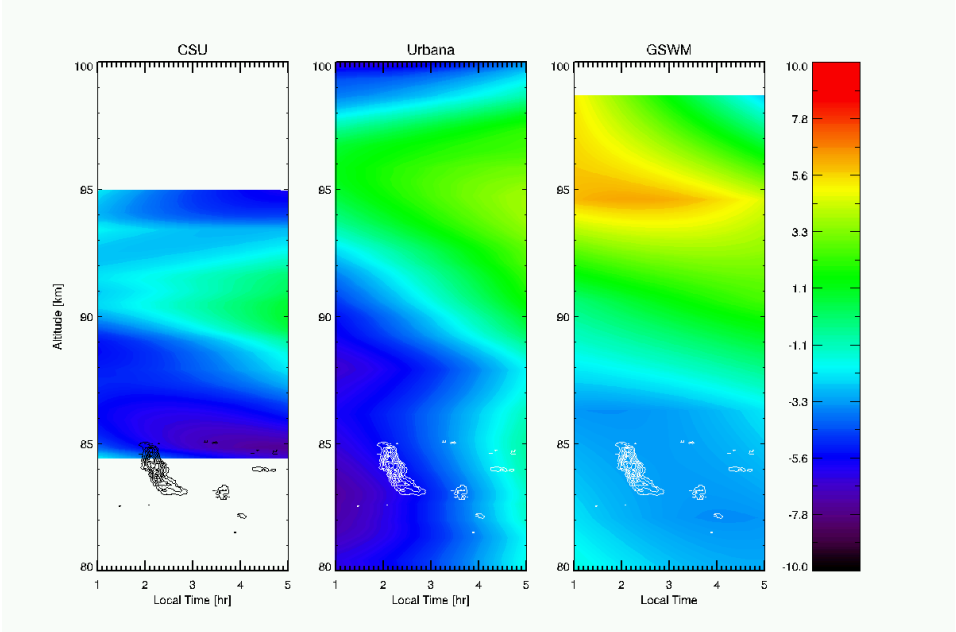

Figure 8 The amplitude of the Diurnal tide measured from the CSU sodium lidar [*She et al.*, 2002] and the sodium lidar at Urbana [*States and Gardner*, 2000] make up the frist two panels. The third panel is the diurnal tide from the GSWM [*Hagan et al.*, 1999; *Hagan et al.*, 2001].

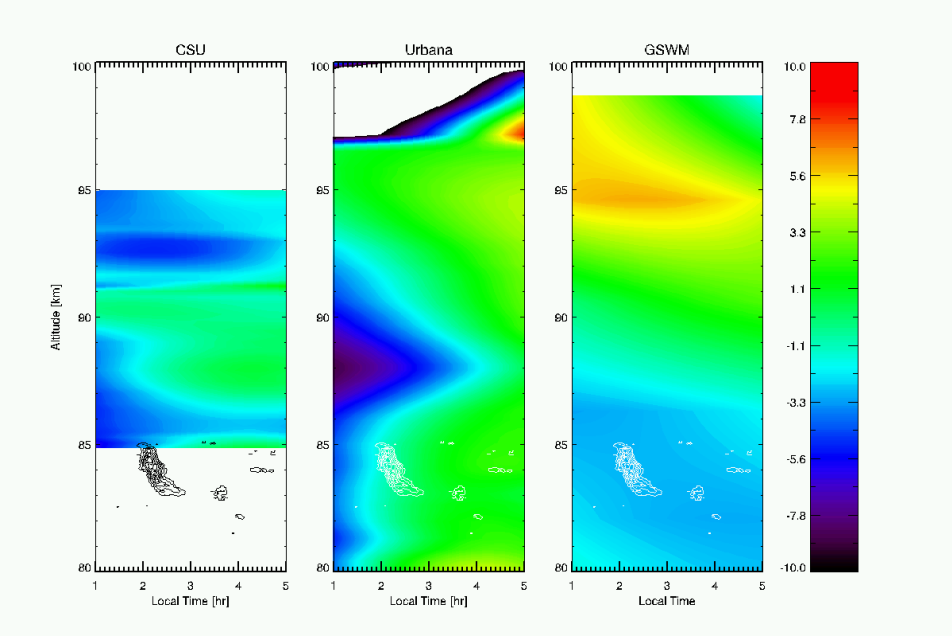

Figure 9 The amplitude of the diurnal and semi-diurnal tide measured from the CSU sodium lidar [*She et al.*, 2002] and the sodium lidar at Urbana [*States and Gardner*, 2000] make up the frist two panels. The third panel is the diurnal and semi-diurnal tide from the GSWM [*Hagan et al.*, 1999; *Hagan et al.*, 2001].

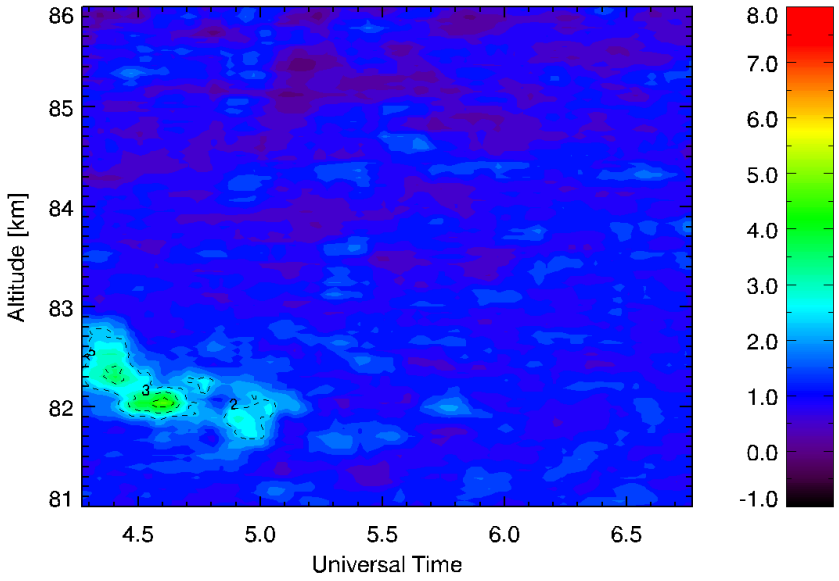

Figure 10 Backscatter ratio of the 1999 NLC [*Wickwar et al.*, 2002].